Author(s): Deppisch, Frank F.; Suhonen, Jouni

Title: Statistical analysis of β decays and the effective value of gA in the proton-neutron quasiparticle random-phase approximation framework

Year: 2016

Version:

Please cite the original version:

Deppisch, F. F., & Suhonen, J. (2016). Statistical analysis of β decays and the effective value of gA in the proton-neutron quasiparticle random-phase approximation framework. Physical Review C, 94(5), Article 055501. https://doi.org/10.1103/PhysRevC.94.055501

Statistical analysis of β decays and the effective value of g_A in the proton-neutron quasiparticle random-phase approximation framework

Frank F. Deppisch*
Department of Physics & Astronomy, University College London, London WC1E 6BT, United Kingdom

Jouni Suhonen†
Department of Physics, University of Jyvaskyla, P.O. Box 35, FI-40014 Jyvaskyla, Finland

(Received 16 June 2016; published 11 November 2016)

We perform a Markov chain Monte Carlo (MCMC) statistical analysis of a number of measured ground-state-to-ground-state single β^+/electron-capture and β^- decays in the nuclear mass range of $A = 62$–142. The corresponding experimental comparative half-lives (log ft values) are compared with the theoretical ones obtained by the use of the proton-neutron quasiparticle random-phase approximation (pnQRPA) with G-matrix-based effective interactions. The MCMC analysis is performed separately for 47 isobaric triplets and 28 more extended isobaric chains of nuclei to extract values and uncertainties for the effective axial-vector coupling constant g_A in nuclear-structure calculations performed in the pnQRPA framework. As far as available, measured half-lives for two-neutrino $\beta\beta^-$ decays occurring in the studied isobaric chains are analyzed as well.

DOI: 10.1103/PhysRevC.94.055501

I. INTRODUCTION

The neutrinoless double-β ($0\nu\beta\beta$) decays of atomic nuclei serve as a forceful incentive to constantly drive nuclear-structure calculations toward better performance. Analyses of the potential experimental $0\nu\beta\beta$ outcomes in the future require accurate knowledge of the related nuclear matrix elements (NMEs) for the obtained data to serve in the best possible ways to unravel the fundamental nature and mass of the neutrino [1–4]. It is also tightly connected to the breaking of lepton number asymmetry and has far reaching consequences even on solutions on the baryon asymmetry of the universe [5,6]. A host of models, ranging from the interacting shell model (ISM) to various mean-field theories, have been used in the calculations. The resulting NMEs have been analyzed in the review article [7]. Most of the calculations have been pursued in the framework of the proton-neutron quasiparticle random-phase approximation (pnQRPA) [8].

In these many calculations it has been noticed that several aspects of nuclear structure make an impact on the resulting values of the NMEs: the chosen valence space and orbital occupancies [9–11], the shell-closure effects [7,12], and the deformation [13–16]. Only lately has the important aspect of the effective value of the axial-vector coupling constant g_A been addressed within a few models like the pnQRPA [17–21], the ISM [22–25], and the interacting boson model 2 (IBA-2) [26].

A particular problem with the pnQRPA calculations, not present in the other calculations, is the unsettled value of the particle-particle interaction parameter $g_{\rm pp}$ describing the strength of the proton-neutron interaction in the 1^+ channel. Since the introduction of this parameter [27,28] it has been attempted to fix its values by the inspection of measured single-β-decay rates [29,30] or $2\nu\beta\beta$-decay rates [31–34].

Here we make an attempt to relate the values of $g_{\rm pp}$ to the values of g_A through the data on β-decay rates associated with the transitions between an even-even nucleus and an odd-odd nucleus. The data on these decays are presented as comparative half-lives (log ft values) and comparing them with the corresponding computed ones one can make conclusions about the possible correlations of these two key parameters of calculation. As a mathematical aid we use the Markov chain Monte Carlo (MCMC) statistical analysis of 47 isobaric triplets and 28 more extended isobaric chains of nuclei. In the isobaric triplets there are two β-decay branches, left and right, between the central and lateral nuclei, and in the extended isobaric chains more complex systems of consecutive central and lateral nuclei can form. To estimate the theoretical uncertainty inherent in the pnQRPA framework we include the full parametric freedom available. This means we introduce an uncertainty in the particle-hole interaction parameter $g_{\rm ph}$. In addition we treat both $g_{\rm pp}$ and $g_{\rm ph}$ as parameters specific only to a given β^+/electron capture (EC) or β^--decay transition pair. This opens up a large parametric freedom that has not been explored before.

Our analysis is intended to address the importance of quenching, i.e., the suppression of g_A with respect to its free value $g_A = 1.269$. Quenched values as low as $g_A \approx 0.4$ have been reported for example in the IBM-2 model [26]; because $0\nu\beta\beta$ decay depends on g_A as $\propto g_A^4$, this could reduce the decay by orders of magnitude, having a serious impact on the observability of $0\nu\beta\beta$ decay in experiments. Whether such strong quenching actually applies to $0\nu\beta\beta$ is not a question we can answer here, because we touch here on only the 1^+ multipolarity of the multipole decomposition of a $0\nu\beta\beta$ decay NME and because the $0\nu\beta\beta$ decay proceeds via a momentum exchange much larger than that of the presently discussed single-β and two-neutrino double-β decays.

The article is organized as follows. In Sec. II the basic theoretical framework is briefly reviewed and the model-space aspects and the adjustment of the model parameters are

*f.deppisch@ucl.ac.uk
†jouni.suhonen@phys.jyu.fi

explained. In Sec. III we make a statistical analysis of the effective value of $g_{\rm A}$. Here we try to chart the possible effective values of the axial-vector coupling constant g_A in model calculations using the *pn*QRPA approach, using different methods. Finally, in Sec. IV, we summarize and draw the conclusions.

II. BRIEF SUMMARY OF THE THEORY

We begin by defining the comparative half-lives ($\log ft$ values) of the $1^+ \leftrightarrow 0^+$ Gamow–Teller transitions that form the basis of the present analysis. The $\log ft$ value is defined as [35]

$$\log ft = \log_{10}(f_0 t_{1/2}[s]) = \log_{10}\left(\frac{6147}{B_{\rm GT}}\right), \tag{1}$$

with

$$B_{\rm GT} = \frac{g_A^2}{2J_i+1}|M_{\rm GT}(g_{\rm pp}, g_{\rm ph})|^2 \tag{2}$$

for the β^+/EC or β^- type of transitions. Here the half-life $t_{1/2}$ has been given in seconds and f_0 is the dimensionless leptonic phase-space factor associated with the process. J_i is the spin of the initial ground state and $M_{\rm GT}$ is the Gamow-Teller NME defined, e.g., in Ref. [35]. Here g_A is the weak axial-vector coupling constant, $g_{\rm pp}$ the particle-particle interaction coupling constant, and $g_{\rm ph}$ the particle-hole interaction coupling constant as defined, e.g., in Refs. [36,37]. Methods of determining the values of these constants are addressed in the next section.

The $2\nu\beta\beta$ decay half-life can be compactly written as

$$\left[t_{1/2}^{(2\nu)}(0_i^+ \to 0_f^+)\right]^{-1} = g_A^4 G_{2\nu}|M^{(2\nu)}|^2, \tag{3}$$

where $G_{2\nu}$ stands for the leptonic phase-space factor without including g_A in the way defined in Ref. [38]. The initial ground state is denoted by 0_i^+ and the final ground state by 0_f^+. The $2\nu\beta\beta$ NME $M^{(2\nu)}$ can be written as

$$M^{(2\nu)} = \sum_{m,n} \frac{M_{\rm F}(1_m^+)\langle 1_m^+|1_n^+\rangle M_{\rm I}(1_n^+)}{D_m}, \tag{4}$$

where the quantity D_m is the energy denominator containing the average energy of the 1^+ states emerging from the *pn*QRPA calculations in the initial and final even-even nuclei. The summation is in general over all intermediate 1^+ states where $\langle 1_m^+|1_n^+\rangle$ is the overlap between two such states. We in general treat the individual matrix elements for the transition between the initial (final) state and the virtual intermediate states, $M_{\rm I(F)}(1_i^+)$, as functions of separate sets of $g_{\rm pp}$ and $g_{\rm ph}$ couplings.

While we do not discuss $0\nu\beta\beta$ decay in detail in this article, we briefly describe the theoretical calculation of the corresponding half-life to illustrate the similarities and differences to the above processes. The $0\nu\beta\beta$-decay half-life can be written as

$$\left[t_{1/2}^{(0\nu)}(0_i^+ \to 0_f^+)\right]^{-1} = g_{A,0\nu}^4 \left(\frac{\langle m_\nu\rangle}{m_e}\right)^2 G_{0\nu}|M^{(0\nu)}|^2, \tag{5}$$

where $G_{0\nu}$ stands for the leptonic phase-space factor without including $g_{A,0\nu}$ and the electron mass m_e in the way defined in Ref. [38]. Here, we denote the effective axial coupling relevant for $0\nu\beta\beta$ decay as $g_{A,0\nu}$ to emphasize that its value may deviate from the one determined in single-β and $2\nu\beta\beta$ decays. The effective $0\nu\beta\beta$ neutrino mass is denoted as $\langle m_\nu\rangle$. As before, the initial ground state is denoted by 0_i^+ and the final ground state by 0_f^+.

The $2\nu\beta\beta$-decay and $0\nu\beta\beta$-decay half-lives share the same strong dependence on g_A as seen in Eqs. (3) and (5). It is thus an essential first step to study the effective value of g_A in single-β and $2\nu\beta\beta$ decays. These studies tangent only the 1^+ contribution to the $0\nu\beta\beta$ decay whereas it is known that higher multipoles are very important for the $0\nu\beta\beta$ decay as well [39]. Some attempts to study these higher multipolarities by way of single-β decays have been made lately [40,41]. It is thus not straightforward to relate the single-β-decay and $2\nu\beta\beta$-decay studies to the value of the $0\nu\beta\beta$ NME, especially since the former involves momentum transfers of a few MeV and the latter involves a virtual neutrino with a momentum exchange of the order of 100 MeV. This allows the possibility that the effective value of g_A gets momentum dependent [24]. Related to this, the high-momentum exchange in $0\nu\beta\beta$ decay makes the higher-J^π states contribute appreciably to the decay rate [42]. For these higher-lying states the quenching of g_A could be different from the low-lying states discussed in the present work. It should be noted, however, that in the *pn*QRPA no closure approximation is imposed in either modes of double-β decay so that the individual contribution from all intermediate states can be accessed in the case of $0\nu\beta\beta$ decay, as well. These intermediate contributions vary strongly from nucleus to nucleus and even some kind of single-state dominance can be observed for some $0\nu\beta\beta$ decaying nuclei [42]. For more details on the theoretical background, we refer the reader to Ref. [20].

In the present calculations we obtain the single-particle energies from a spherical Coulomb-corrected Woods-Saxon (WS) potential with the standard parametrization of Bohr and Mottelson [43]. This parametrization is optimized for nuclei near the line of β stability and is thus well suited for the presently studied nuclei. The single-particle orbitals used in the calculations span the space $0f$-$1p$-$0g$-$2s$-$1d$-$0h_{11/2}$ for the masses $A = 62$–80, $0f$-$1p$-$0g$-$2s$-$1d$-$0h$ for the masses $A = 98$–108, and $0f$-$1p$-$0g$-$2s$-$1d$-$0h$-$1f$-$2p$ for the masses $A = 110$–142. In these single-particle bases the proton and neutron Fermi surfaces are well contained in the model space. The Bonn-A G matrix has been used as the starting point for the nucleon-nucleon interaction and it has been renormalized in the standard way [37,44]: The quasiparticles are treated in the BCS formalism and the pairing matrix elements are scaled by a common strength parameter, separately for protons and neutrons. In practice these factors are fitted such that the lowest quasiparticle energies obtained from the BCS match the experimentally deduced pairing gaps for protons and neutrons, respectively. For closed major shells the pairing strength parameters were taken from the closest even-even neighbor.

The wave functions of the 1^+ states of the intermediate nuclei have been produced by using the *pn*QRPA with the particle-hole and particle-particle degrees of freedom (DOF) [27] included. The particle-hole and particle-particle parts of the proton-neutron two-body interaction are separately scaled

by the $g_{\rm ph}$ and $g_{\rm pp}$ parameters. The particle-hole parameter affects the position of the Gamow-Teller giant resonance (GTGR) in the odd-odd nucleus and its value is fixed by the available systematics [35] on the location of the resonance:

$$\begin{aligned}\Delta E_{\rm GT} &= E(1^+_{\rm GTGR}) - E(0^+_{\rm gs}) \\ &= [1.444(Z+1/2)A^{-1/3} - 30.0(N-Z-2)A^{-1} \\ &\quad + 5.57]\,{\rm MeV}. \end{aligned} \tag{6}$$

The difference $\Delta E_{\rm GT}$ between the GTGR and the ground state of the neighboring even-even reference nucleus thus depends on the proton and neutron numbers (Z,N) of the reference nucleus, as well as on its mass number. In practice, both the measured and the computed GTGRs have a width and their locations are determined by the centroid (weighted average) of the strengths associated with the individual 1^+ states comprising the GTGR. In a *pn*QRPA calculation the difference $E(1^+_{\rm GTGR}) - E(0^+_{\rm gs})$ in Eq. (6) gives the empirical location of the centroid of the GTGR, which has to be matched by the centroid of the *pn*QRPA computed strengths of the 1^+ states presumed to belong to the GTGR. The computed centroid depends strongly on the value of the $g_{\rm ph}$ parameter and weakly on the choice of the set of 1^+ states included in the GTGR, the latter introducing an inherent source of error. Throughout our calculations we assume that the value of $g_{\rm ph}$ in a given system is determined with a relative error of 15% as a source of theoretical uncertainty. This 15% error represents a maximum deviation in $g_{\rm ph}$ such that the computed centroid of the Gamow-Teller giant resonance is not meaninglessly far from its empirical position as given by Eq. (6). Throughout we denote with $\gamma_{\rm ph}$ the normalized value of the particle-hole parameter with respect to the value determined through the GTGR. The determination of the values of $g_{\rm pp}$, together with the axial-vector coupling constant g_A, is presented below.

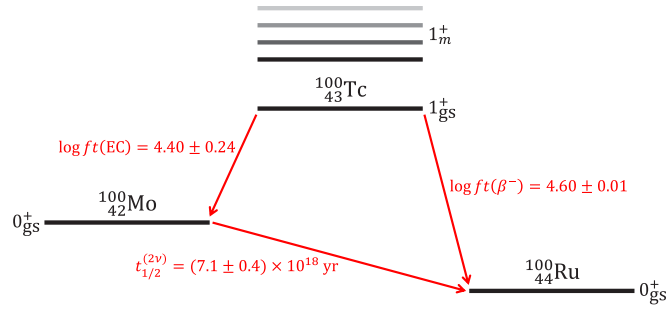

FIG. 1. Double- and single-β-decay characteristics of the isobaric triplet $^{100}_{42}$Mo, $^{100}_{43}$Tc, and $^{100}_{44}$Ru. The experimental $2\nu\beta\beta$ half-lives and the log ft values are discussed in Sec. III.

As an example, Fig. 1 schematically shows the energy levels and decay characteristics of a triplet of isobars: $^{100}_{42}$Mo, $^{100}_{43}$Tc, and $^{100}_{44}$Ru. Figure 2(a) displays the nuclear matrix elements of the single-β decays $^{100}_{43}{\rm Tc} \to {}^{100}_{42}{\rm Mo}$ and $^{100}_{43}{\rm Tc} \to {}^{102}_{44}{\rm Ru}$ and the $2\nu\beta\beta$ decay $^{102}_{42}{\rm Mo} \to {}^{102}_{44}{\rm Ru}$ as functions of $g_{\rm pp}$. The 1σ and 2σ uncertainties due to a variation of the parameter $g_{\rm ph}$ around its value determined by the GTGR are shown using the colored bands. The dependence of the single-β NMEs shows a typical behavior seen in many triplets where one NME increases whereas the other decreases. This has the effect that the dependence of the product of the NMEs on $g_{\rm pp}$ can become rather weak and consequently the value of g_A can be extracted from the product of the log ft values separately. This behavior is not universal, as exemplified in Fig. 2(b) showing the NMEs of the processes $^{68}_{31}{\rm Ga} \to {}^{68}_{30}{\rm Zn}$ and $^{68}_{32}{\rm Ge} \to {}^{68}_{31}{\rm Ga}$ ($2\nu\beta\beta$ decay

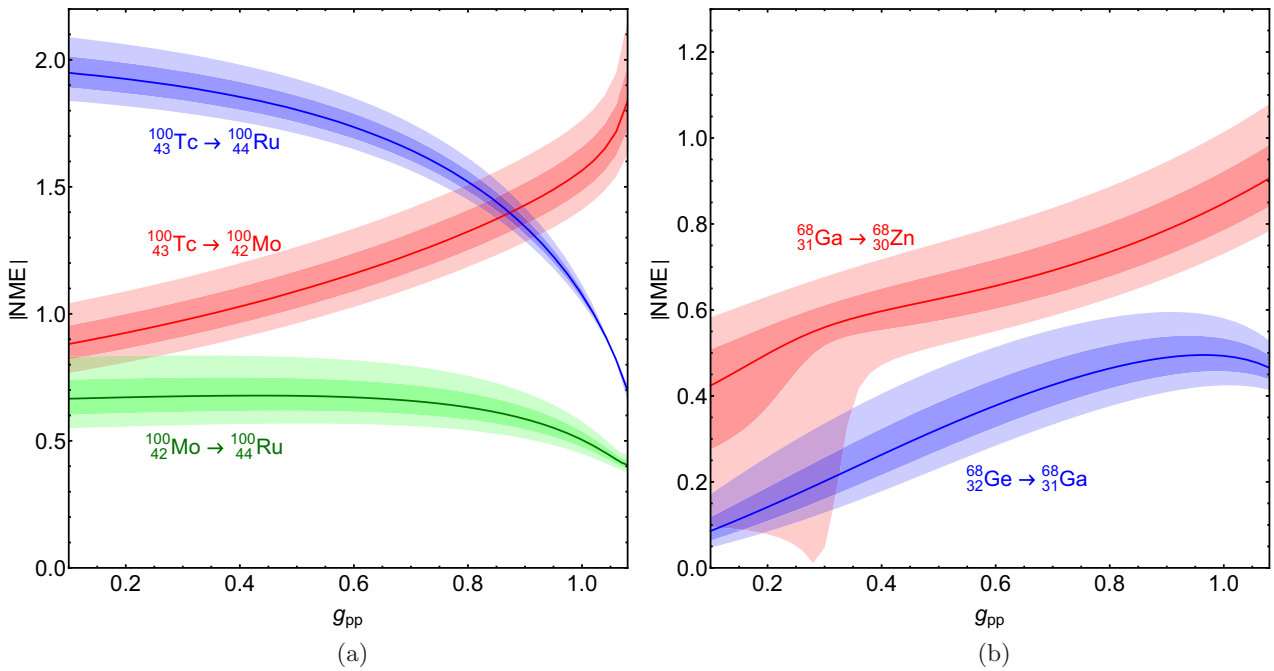

FIG. 2. (a) Nuclear matrix elements for the single-β decays $^{100}_{43}{\rm Tc} \to {}^{100}_{42}{\rm Mo}$ (red) and $^{100}_{43}{\rm Tc} \to {}^{102}_{44}{\rm Ru}$ (blue) and the $2\nu\beta\beta$ decay $^{102}_{42}{\rm Mo} \to {}^{102}_{44}{\rm Ru}$ (green) as a function of $g_{\rm pp}$. The colored bands show the uncertainty of the matrix elements with a 15% variation and a 30% variation of $g_{\rm ph}$ around its value derived from the GTGR. (b) As before but for the single-β decays $^{68}_{31}{\rm Ga} \to {}^{68}_{30}{\rm Zn}$ (red) and $^{68}_{32}{\rm Ge} \to {}^{68}_{31}{\rm Ga}$ (blue).

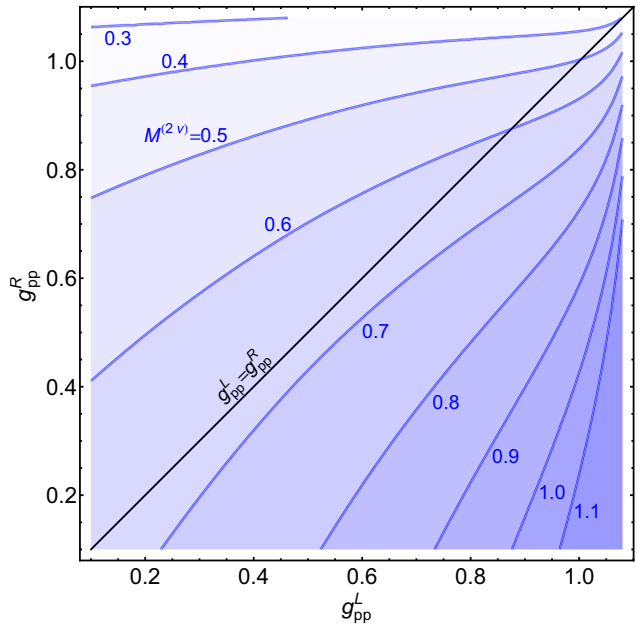

FIG. 3. Nuclear matrix element for the $2\nu\beta\beta$ decay $^{100}_{42}$Mo $\rightarrow$ $^{100}_{44}$Ru as a function of the left-leg and right-leg particle-particle parameters g^L_{pp} and g^R_{pp}, respectively. The isocurves indicate constant NME values as shown. The particle-hole parameters are set at their GTGR values, $\gamma^L_{ph} = \gamma^R_{ph} = 1$.

is not possible here). Here, both NMEs rise with g_{pp}, which will couple the determination of g_A and g_{pp} as is discussed in Sec. III. As can be seen, a variation of g_{ph} at the 15% level generically has an effect on the matrix elements of the same order, depending on the isotopes involved.

In Fig. 2 both the left-leg and the right-leg NMEs were treated as depending on the same g_{pp} as is assumed in most analyses. As discussed above, we in turn treat the transitions independently, each depending on separate parameters, g^L_{pp} and g^R_{pp}. This has the immediate effect that the β-decay/EC processes become statistically independent because they now depend on different parameters. In addition, the NME of the $2\nu\beta\beta$ decay (if allowed within a given triplet) now becomes a function of both g^L_{pp} and g^R_{pp}. Figure 3 illustrates the dependence of the NME for the $2\nu\beta\beta$ decay $^{102}_{42}$Mo $\rightarrow$ $^{102}_{44}$Ru. The isocurves indicate constant values for the NME as shown. The plot demonstrates that the left-leg and right-leg NMEs are correlated such that the $2\nu\beta\beta$ remains approximately constant if both depend on the same $g_{pp} \lesssim 0.7$ [along the diagonal, also compare with Fig. 2(a)]. This degeneracy is lifted if g^L_{pp} and g^R_{pp} are allowed to vary independently. The dependence on the particle-hole parameters, which we in turn also treat as independent values, is neglected, and they are set at their GTGR values, $\gamma^L_{ph} = \gamma^R_{ph} = 1$.

III. STATISTICAL ANALYSIS

A. Quenching of the axial-vector coupling constant

At this stage it is worth pointing to some other earlier works devoted to the determination of the effective value of g_A in calculations using the *pn*QRPA model or other models. A strongly reduced effective value of $g_A \approx 0.6$ was reported in the shell-model calculations [45] in the mass $A = 90$–97 region. In a more recent shell-model study [25] values of about $g_A \sim 0.7$ were obtained in the mass regions $A = 128$ and 130 and an even stronger quenching of $g_A = 0.56$ was obtained for $A = 136$. The first analysis performed in the *pn*QRPA model was done in Ref. [17] where both the β-decay and the $2\nu\beta\beta$-decay data were analyzed for the $A = 100$ and 116 systems using a least-squares fit to determine the values $g_A = 0.74$ ($A = 100$) and $g_A = 0.84$ ($A = 116$). It is interesting to note that in the first version [46] of Ref. [17] also the result $g_A = 0.39$ for the $A = 128$ system was quoted. An approximately monotonic behavior of the effective values of g_A was parametrized in Ref. [26] by analyzing the magnitudes of NMEs produced by the IBA-2 model. Values around $g_A = 0.5$ were obtained. In a later publication [47] the interacting boson-fermion-fermion model, IBFFM-2, was adopted and the subsequent analyses yielded highly suppressed values of $g_A \approx 0.3$ for the $A = 128$ nuclei. Recently a systematic approach to β and $2\nu\beta\beta$ decays in the mass region $A = 100$–136 was performed [48]. The suitability to the description of the global behavior of the β and $2\nu\beta\beta$ decays, a linear model and an overall-quenched $g_A \approx 0.6$ were examined. The present study is an extension of this work as well as Refs. [18,20,29] to a wider mass region and a refinement in the statistical analysis methods used to extract information on the quenching of g_A in this wider region.

The apparently low effective values of g_A in the *pn*QRPA could be attributed to missing the contributions of the complex configurations beyond the two-quasiparticle (particle-hole) configurations of the *pn*QRPA (see also Ref. [19]). On the other hand, it was shown in Ref. [49] for the $2\nu\beta\beta$ decay of ^{76}Ge and in Ref. [50] for the $2\nu\beta\beta$ decay of ^{100}Mo that the inclusion of the four-quasiparticle (two-particle–two-hole) degrees of freedom in a higher-QRPA scheme [in this case the proton-neutron microscopic anharmonic vibrator approach (*pn*MAVA)] does not affect appreciably the low-energy Gamow-Teller properties of *pn*QRPA. It is yet unclear what is the primary reason for the rather low effective values of g_A and what is the share between the model-dependent and model-independent contributions to it. The model-independent quenching can be associated with the non-nucleonic, i.e., isobaric degrees of freedom in nuclear matter [51,52]. Contributions to the model-dependent quenching come from the limitations in the single-particle models' space (ISM, IBA-2, IBFFM-2) or the lack of complicated many-nucleon configurations (*pn*QRPA, IBA-2, IBFFM-2). The determination of the effective values of g_A in different theory frameworks is an extremely interesting issue and certainly necessitates further investigation in the future.

B. Fitting isobaric triplets

The basis of our analyses is provided by the experimental $\log ft$ values of the relevant β decays/EC processes. They are shown in Tables I and II, displaying the comparative half-lives $\log ft_L$ and $\log ft_R$ for the left-leg decay and the right-leg decay of a given triplet. The comparative half-lives were calculated from the experimentally measured half-lives listed in Ref. [53] incorporating the experimental uncertainty in both the measured decay half-life and the Q value. In most

TABLE I. Characteristics of the β^+/EC and β^- decays in isobaric triplets within the mass range $A = 62$–114 studied in the present article. An isobaric triplet is identified by the mass number A and the lowest atomic number Z_0 among the three isotopes. The isotopes in the triplets are indicated along with their spin J and parity π (J^π). The arrows denote the direction of the relevant β^+/EC, β^- decay. The experimentally determined comparative half-lives of the left transition and the right transition are given as $\log ft_L$ and $\log ft_R$, respectively. $2\nu\beta\beta$ decaying isotopes are underlined. The values of g_A and $g_{\rm pp}$ are determined in the triplet fit described in Sec. III B. Cases in which the best-fit $\chi^2_{\rm min}$ is in the range [0.5,2.2], indicating slight incompatibility with data, are highlighted with italic numbers. Cases with stronger discrepancy are highlighted in bold. In all other cases a $\chi^2_{\rm min} = 0$ (within numerical tolerance) was found.

A	Z_0	Triplet	$\log ft_L^{\rm exp}$	$\log ft_R^{\rm exp}$	$g_A^{\rm fit}$	$g_{\rm pp}^{\rm fit}$
62	28	$\mathrm{Ni}(0^+) \leftarrow \mathrm{Cu}(1^+) \leftarrow \mathrm{Zn}(0^+)$	5.1521 ± 0.0014	5.0117 ± 0.0010	$0.75^{+0.21}_{-0.01}$	$1.10^{+0.01}_{-0.40}$
64	28	$\mathrm{Ni}(0^+) \leftarrow \mathrm{Cu}(1^+) \rightarrow \mathrm{Zn}(0^+)$	4.9931 ± 0.0022	5.3095 ± 0.0038	$\mathit{0.81}^{+0.11}_{-0.04}$	$\mathit{0.92}^{+0.09}_{-0.19}$
66	28	$\mathrm{Ni}(0^+) \rightarrow \mathrm{Cu}(1^+) \rightarrow \mathrm{Zn}(0^+)$	4.2754 ± 0.0094	5.3394 ± 0.0013	$0.93^{+0.24}_{-0.01}$	$0.82^{+0.04}_{-0.34}$
68	29	$\mathrm{Cu}(1^+) \rightarrow \mathrm{Zn}(0^+) \leftarrow \mathrm{Ga}(1^+)$	5.7716 ± 0.0085	5.1918 ± 0.0012	$0.70^{+0.06}_{-0.09}$	$0.19^{+0.02}_{-0.01}$
68	30	$\mathrm{Zn}(0^+) \leftarrow \mathrm{Ga}(1^+) \leftarrow \mathrm{Ge}(0^+)$	5.1918 ± 0.0012	4.9955 ± 0.0224	$\mathit{0.50}^{+0.08}_{-0.04}$	$\mathit{0.78}^{+0.13}_{-0.21}$
70	29	$\mathrm{Cu}(1^+) \rightarrow \underline{\mathrm{Zn}}(0^+) \leftarrow \mathrm{Ga}(1^+)$	5.4317 ± 0.0138	4.7443 ± 0.0640		
70	30	$\underline{\mathrm{Zn}}(0^+) \leftarrow \mathrm{Ga}(1^+) \rightarrow \mathrm{Ge}(0^+)$	4.7443 ± 0.0640	5.1021 ± 0.0018	$1.10^{+0.13}_{-0.26}$	$0.43^{+0.29}_{-0.15}$
78	34	$\mathrm{Se}(0^+) \leftarrow \mathrm{Br}(1^+) \rightarrow \mathrm{Kr}(0^+)$	4.7460 ± 0.0040	$>5.50 \pm 0.01$	$0.42^{+0.02}_{-0.04}$	$1.00^{+0.04}_{-0.02}$
80	33	$\mathrm{As}(1^+) \rightarrow \underline{\mathrm{Se}}(0^+) \leftarrow \mathrm{Br}(1^+)$	5.7460 ± 0.0099	4.6868 ± 0.0123	$0.98^{+0.21}_{-0.08}$	$0.34^{+0.04}_{-0.11}$
80	34	$\underline{\mathrm{Se}}(0^+) \leftarrow \mathrm{Br}(1^+) \rightarrow \mathrm{Kr}(0^+)$	4.6868 ± 0.0123	5.4953 ± 0.0024	$\mathit{0.90}^{+0.33}_{-0.07}$	$\mathit{0.48}^{+0.06}_{-0.23}$
80	35	$\mathrm{Br}(1^+) \rightarrow \mathrm{Kr}(0^+) \leftarrow \mathrm{Rb}(1^+)$	5.4953 ± 0.0024	4.9208 ± 0.0514	**1.40**	**0.27**
98	39	$\mathrm{Y}(1^+) \rightarrow \mathrm{Zr}(0^+) \rightarrow \mathrm{Nb}(1^+)$	5.3740 ± 0.1660	4.1762 ± 0.0170	$0.53^{+0.05}_{-0.03}$	$0.68^{+0.06}_{-0.11}$
100	41	$\mathrm{Nb}(1^+) \rightarrow \underline{\mathrm{Mo}}(0^+) \leftarrow \mathrm{Tc}(1^+)$	5.1622 ± 0.0586	4.4047 ± 0.2414	$0.61^{+0.14}_{-0.15}$	$0.89^{+0.06}_{-0.08}$
100	42	$\underline{\mathrm{Mo}}(0^+) \leftarrow \mathrm{Tc}(1^+) \rightarrow \mathrm{Ru}(0^+)$	4.4047 ± 0.2414	4.6063 ± 0.0054	$0.56^{+0.09}_{-0.12}$	$0.96^{+0.05}_{-0.16}$
102	42	$\mathrm{Mo}(0^+) \rightarrow \mathrm{Tc}(1^+) \rightarrow \mathrm{Ru}(0^+)$	4.2079 ± 0.0362	4.8001 ± 0.0129	$0.41^{+0.02}_{-0.02}$	$0.68^{+0.05}_{-0.06}$
104	44	$\underline{\mathrm{Ru}}(0^+) \leftarrow \mathrm{Rh}(1^+) \rightarrow \mathrm{Pd}(0^+)$	4.3246 ± 0.1030	4.5555 ± 0.0056	$0.59^{+0.05}_{-0.07}$	$0.92^{+0.03}_{-0.06}$
106	45	$\mathrm{Rh}(1^+) \rightarrow \mathrm{Pd}(0^+) \leftarrow \mathrm{Ag}(1^+)$	5.1899 ± 0.0060	4.9148 ± 0.0035	$0.40^{+0.02}_{-0.02}$	$0.87^{+0.01}_{-0.01}$
106	46	$\mathrm{Pd}(0^+) \leftarrow \mathrm{Ag}(1^+) \rightarrow \mathrm{Cd}(0^+)$	4.9148 ± 0.0035	$> 4.18 \pm 0.25$	$0.36^{+0.25}_{-0.04}$	$1.00^{+0.13}_{-0.72}$
108	44	$\mathrm{Ru}(0^+) \rightarrow \mathrm{Rh}(1^+) \rightarrow \mathrm{Pd}(0^+)$	4.4885 ± 0.0223	5.5440 ± 0.0480	$0.27^{+0.01}_{-0.02}$	$0.69^{+0.04}_{-0.06}$
108	45	$\mathrm{Rh}(1^+) \rightarrow \mathrm{Pd}(0^+) \leftarrow \mathrm{Ag}(1^+)$	5.5440 ± 0.0480	4.7085 ± 0.0372	$0.43^{+0.03}_{-0.05}$	$0.86^{+0.19}_{-0.01}$
108	46	$\mathrm{Pd}(0^+) \leftarrow \mathrm{Ag}(1^+) \rightarrow \mathrm{Cd}(0^+)$	4.7085 ± 0.0372	4.4410 ± 0.0080	$0.49^{+0.02}_{-0.02}$	$0.67^{+0.05}_{-0.08}$
110	46	$\underline{\mathrm{Pd}}(0^+) \leftarrow \mathrm{Ag}(1^+) \rightarrow \mathrm{Cd}(0^+)$	4.0963 ± 0.0887	4.6762 ± 0.0021	$0.77^{+0.06}_{-0.08}$	$0.87^{+0.02}_{-0.04}$
112	48	$\mathrm{Cd}(0^+) \leftarrow \mathrm{In}(1^+) \rightarrow \mathrm{Sn}(0^+)$	4.6342 ± 0.0378	4.1515 ± 0.0497	$0.70^{+0.04}_{-0.03}$	$0.61^{+0.07}_{-0.11}$
114	46	$\mathrm{Pd}(0^+) \rightarrow \mathrm{Ag}(1^+) \rightarrow \mathrm{Cd}(0^+)$	4.2124 ± 0.0153	5.1008 ± 0.0096	$0.51^{+0.03}_{-0.03}$	$0.49^{+0.06}_{-0.09}$
114	47	$\mathrm{Ag}(1^+) \rightarrow \underline{\mathrm{Cd}}(0^+) \leftarrow \mathrm{In}(1^+)$	5.1008 ± 0.0096	4.8877 ± 0.1470	$0.54^{+0.06}_{-0.07}$	$0.54^{+0.08}_{-0.13}$
114	48	$\underline{\mathrm{Cd}}(0^+) \leftarrow \mathrm{In}(1^+) \rightarrow \mathrm{Sn}(0^+)$	4.8877 ± 0.1470	4.4856 ± 0.0010	$\mathit{0.61}^{+0.06}_{-0.01}$	$\mathit{0.46}^{+0.15}_{-0.01}$

cases, the experimental uncertainty is negligible compared to the theoretical uncertainties expected to be inherent in nuclear model calculation; the errors in the values of the comparative half-lives range between the per mil and the 10% level. In two cases only, a lower limit is known. The range of considered isotopes is dictated by the applicability of the theory framework (the quasiparticle description for s-d shell nuclei becomes questionable for lighter nuclei) and nature (for example, the 1^+ states are not the ground states in the odd-odd systems in the mass gaps $A = 72$–76 and $A = 82$–96).

As far as available and relevant for our selection of isotopes we also calculate the $2\nu\beta\beta$-decay half-lives. The characteristics of $2\nu\beta\beta$ decaying isotopes are shown in Table III giving the phase-space factor $G_{2\nu}$ and the experimental half-lives for three of the isotopes. The fitted or predicted half-lives are discussed below.

We start by fitting the triplets individually, i.e., we compare the theoretically predicted $\log ft$ values of the left-leg and right-leg decays in a triplet of Tables I and II with the experimental data. For this purpose, we assume that both decays depend on the same pair: g_A, $g_{\rm pp}$. In addition we also include a variation of the $g_{\rm ph}$ couplings independently for each decay, with a 1σ deviation of 15% from its GTGR value.

Because we later work with a larger number of free parameters and in systems that can be underconstrained, exactly constrained, or overconstrained, we consistently perform the fitting procedure using a straightforward MCMC based on the Metropolis-Hastings algorithm [55]. Throughout our calculations, we have verified that the uncertainties inherent in the MCMC due to finite sampling, etc., are small compared to the physical uncertainties. We always use a flat prior in the given fitting parameters; i.e., they are randomly selected on a

TABLE II. Same as Table I, but for isobaric triplets in the mass range $A = 116$–142.

A	Z_0	Triplet	$\log ft_L^{\rm exp}$	$\log ft_R^{\rm exp}$	$g_A^{\rm fit}$	$g_{\rm pp}^{\rm fit}$
116	48	$\underline{\rm Cd}(0^+) \leftarrow {\rm In}(1^+) \rightarrow {\rm Sn}(0^+)$	4.4508 ± 0.1160	4.6839 ± 0.0025	$0.84^{+0.08}_{-0.08}$	$0.65^{+0.07}_{-0.11}$
118	48	${\rm Cd}(0^+) \rightarrow {\rm In}(1^+) \rightarrow {\rm Sn}(0^+)$	3.9218 ± 0.0629	4.8147 ± 0.0263	$0.88^{+0.09}_{-0.07}$	$0.75^{+0.04}_{-0.09}$
118	49	${\rm In}(1^+) \rightarrow {\rm Sn}(0^+) \leftarrow {\rm Sb}(1^+)$	4.8147 ± 0.0263	4.5152 ± 0.0122	$0.77^{+0.05}_{-0.06}$	$0.65^{+0.03}_{-0.04}$
118	50	${\rm Sn}(0^+) \leftarrow {\rm Sb}(1^+) \leftarrow {\rm Te}(0^+)$	4.5152 ± 0.0122	4.9749 ± 0.0579	$0.77^{+0.06}_{-0.05}$	$0.65^{+0.04}_{-0.14}$
120	48	${\rm Cd}(0^+) \rightarrow {\rm In}(1^+) \rightarrow {\rm Sn}(0^+)$	4.0996 ± 0.0433	5.0483 ± 0.0183	$0.74^{+0.07}_{-0.05}$	$0.77^{+0.04}_{-0.08}$
120	49	${\rm In}(1^+) \rightarrow {\rm Sn}(0^+) \leftarrow {\rm Sb}(1^+)$	5.0483 ± 0.0183	4.5220 ± 0.0048	$0.71^{+0.06}_{-0.06}$	$0.74^{+0.03}_{-0.03}$
122	48	${\rm Cd}(0^+) \rightarrow {\rm In}(1^+) \rightarrow \underline{\rm Sn}(0^+)$	3.9717 ± 0.0451	5.1362 ± 0.0894	$0.82^{+0.09}_{-0.06}$	$0.85^{+0.05}_{-0.08}$
122	52	${\rm Te}(0^+) \leftarrow {\rm I}(1^+) \leftarrow {\rm Xe}(0^+)$	4.9323 ± 0.0077	5.1804 ± 0.0154	$0.50^{+0.04}_{-0.03}$	$0.60^{+0.05}_{-0.12}$
122	53	${\rm I}(1^+) \leftarrow {\rm Xe}(0^+) \leftarrow {\rm Cs}(1^+)$	5.1804 ± 0.0154	5.3606 ± 0.0102	$0.43^{+0.04}_{-0.03}$	$0.36^{+0.02}_{-0.02}$
124	54	${\rm Xe}(0^+) \leftarrow {\rm Cs}(1^+) \leftarrow {\rm Ba}(0^+)$	5.0750 ± 0.0080	5.2074 ± 0.0216	$0.39^{+0.03}_{-0.02}$	$0.71^{+0.03}_{-0.06}$
126	54	${\rm Xe}(0^+) \leftarrow {\rm Cs}(1^+) \leftarrow {\rm Ba}(0^+)$	5.0492 ± 0.0084	5.3577 ± 0.0135	$0.44^{+0.03}_{-0.03}$	$0.67^{+0.04}_{-0.08}$
128	52	$\underline{\rm Te}(0^+) \leftarrow {\rm I}(1^+) \rightarrow {\rm Xe}(0^+)$	5.0439 ± 0.0514	6.0825 ± 0.0055	$0.55^{+0.08}_{-0.03}$	$0.10^{+0.26}_{-0.05}$
128	53	${\rm I}(1^+) \rightarrow {\rm Xe}(0^+) \leftarrow {\rm Cs}(1^+)$	6.0825 ± 0.0055	4.8255 ± 0.0036	$0.68^{+0.09}_{-0.07}$	$0.43^{+0.01}_{-0.01}$
128	54	${\rm Xe}(0^+) \leftarrow {\rm Cs}(1^+) \leftarrow {\rm Ba}(0^+)$	4.8255 ± 0.0036	5.3973 ± 0.0235	$0.58^{+0.05}_{-0.05}$	$0.65^{+0.04}_{-0.09}$
130	54	${\rm Xe}(0^+) \leftarrow {\rm Cs}(1^+) \rightarrow {\rm Ba}(0^+)$	5.0654 ± 0.0049	5.1314 ± 0.0692	**0.78**	**0.10**
134	56	${\rm Ba}(0^+) \leftarrow {\rm La}(1^+) \leftarrow {\rm Ce}(0^+)$	4.8703 ± 0.0154	5.1920 ± 0.0790	$0.73^{+0.07}_{-0.06}$	$0.34^{+0.12}_{-0.13}$
138	58	${\rm Ce}(0^+) \leftarrow {\rm Pr}(1^+) \leftarrow {\rm Nd}(0^+)$	4.5880 ± 0.0160	5.0934 ± 0.0422	$0.98^{+0.08}_{-0.08}$	$0.47^{+0.07}_{-0.14}$
140	58	${\rm Ce}(0^+) \leftarrow {\rm Pr}(1^+) \leftarrow {\rm Nd}(0^+)$	4.4064 ± 0.0035	5.4279 ± 0.0643	$1.00^{+0.09}_{-0.07}$	$0.46^{+0.07}_{-0.16}$
140	59	${\rm Pr}(1^+) \leftarrow {\rm Nd}(0^+) \leftarrow {\rm Pm}(1^+)$	5.4279 ± 0.0643	4.3085 ± 0.0129	$1.30^{+0.06}_{-0.15}$	$0.61^{+0.02}_{-0.03}$
140	60	${\rm Nd}(0^+) \leftarrow {\rm Pm}(1^+) \leftarrow {\rm Sm}(0^+)$	4.3085 ± 0.0129	4.8933 ± 0.0214	$1.20^{+0.08}_{-0.09}$	$0.66^{+0.04}_{-0.08}$
140	61	${\rm Pm}(1^+) \leftarrow {\rm Sm}(0^+) \leftarrow {\rm Eu}(1^+)$	4.8933 ± 0.0214	4.3916 ± 0.0142	$1.20^{+0.10}_{-0.13}$	$0.67^{+0.01}_{-0.01}$
140	62	${\rm Sm}(0^+) \leftarrow {\rm Eu}(1^+) \leftarrow {\rm Gd}(0^+)$	4.3916 ± 0.0142	4.5357 ± 0.0266	$1.10^{+0.08}_{-0.07}$	$0.74^{+0.03}_{-0.07}$
142	60	${\rm Nd}(0^+) \leftarrow {\rm Pm}(1^+) \leftarrow {\rm Sm}(0^+)$	4.4687 ± 0.0183	5.1656 ± 0.0151	$1.00^{+0.08}_{-0.06}$	$0.45^{+0.08}_{-0.12}$
142	61	${\rm Pm}(1^+) \leftarrow {\rm Sm}(0^+) \leftarrow {\rm Eu}(1^+)$	5.1656 ± 0.0151	4.2736 ± 0.0239	$1.30^{+0.03}_{-0.17}$	$0.67^{+0.01}_{-0.02}$

TABLE III. Characteristics of $2\nu\beta\beta$ isotopes studied in the present article. The phase-space factors $G_{2\nu}$ were calculated using the formalism of Ref. [1]. The experimental half-lives were reported in Ref. [54]. The theoretically determined values $[t_{1/2}^{(2\nu)}]_{\rm triplet}$ and $[t_{1/2}^{(2\nu)}]_{\rm multiplet}$ are the *predictions* for the $2\nu\beta\beta$ half-lives based on the triplet and multiplet single-β/EC fits described in Secs. III B and III C, respectively. The italicized half-lives are derived in multiplet fits with a slight tension between data and theory. For ^{70}Zn and ^{80}Se, no meaningful multiplet result could be derived due to the insufficient quality of the underlying fits.

A	Z	Isotope	$G_{2\nu}$ (yr^{-1})	$[t_{1/2}^{(2\nu)}]_{\rm exp}$ (yr)	$[t_{1/2}^{(2\nu)}]_{\rm triplet}$ (yr)	$[t_{1/2}^{(2\nu)}]_{\rm multiplet}$ (yr)
70	30	Zn	1.24×10^{-22}		$(7.0 \pm 4.1) \times 10^{22}$	
80	34	Se	7.06×10^{-29}		$(2.6 \pm 1.7) \times 10^{29}$	
100	42	Mo	3.87×10^{-18}	$(0.71 \pm 0.04) \times 10^{19}$	$(1.1 \pm 0.6) \times 10^{19}$	$(1.5 \pm 0.6) \times 10^{19}$
104	44	Ru	3.80×10^{-21}		$(7.8 \pm 1.7) \times 10^{21}$	$(4.3 \pm 3.7) \times 10^{21}$
110	46	Pd	1.64×10^{-19}		$(1.5 \pm 0.3) \times 10^{20}$	$(1.3 \pm 0.4) \times 10^{20}$
114	48	Cd	6.09×10^{-24}		$(7.0 \pm 1.2) \times 10^{24}$	$(7.5 \pm 1.2) \times 10^{24}$
116	48	Cd	3.27×10^{-18}	$(2.85 \pm 0.15) \times 10^{19}$	$(1.3 \pm 0.3) \times 10^{19}$	$(1.2 \pm 0.3) \times 10^{19}$
122	50	Sn	4.45×10^{-25}	-	$(2.2 \pm 2.0) \times 10^{27}$	$(1.7 \pm 0.7) \times 10^{27}$
128	52	Te	3.61×10^{-22}	$(2.00 \pm 0.30) \times 10^{24}$	$(0.8 \pm 0.2) \times 10^{24}$	$(1.0 \pm 0.2) \times 10^{24}$

linear scale within a given range. We always vary g_A and g_{pp} in the range [0.1,1.4] and γ_{ph} between [0.5,1.5].

In the current case, the fitting is based on a χ^2 function applied to a given triplet of the form

$$\chi^2(g_A,g_{pp},\gamma_{ph}^L,\gamma_{ph}^R) = \left(\frac{\log ft_L^{th}(g_A,g_{pp},\gamma_{ph}^L) - \log ft_L^{exp}}{\delta \log ft_L^{exp}}\right)^2 + \left(\frac{\log ft_R^{th}(g_A,g_{pp},\gamma_{ph}^R) - \log ft_R^{exp}}{\delta \log ft_R^{exp}}\right)^2 + \left(\frac{\gamma_{ph}^L - 1}{\delta\gamma_{ph}^L}\right)^2 \left\{ + \left(\frac{\gamma_{ph}^R - 1}{\delta\gamma_{ph}^R}\right)^2 \right\}. \quad (7)$$

Here, the experimental $\log ft_{L,R}^{exp}$ values along with their experimental errors $\delta \log ft_{L,R}^{exp}$ are taken from Tables I and II. The theoretically determined $\log ft_{L,R}^{th}$ are computed as functions of the fitting parameters g_A and g_{pp}. In addition, they depend on the variables $\gamma_{ph}^{L,R}$, which represent the particle-hole parameters relative to values as derived from the energy of the giant resonance, $\gamma_{ph}^{L,R} = g_{ph}^{L,R}/[g_{ph}^{L,R}]_{GTGR}$. The last two terms in Eq. (7) correspond to using the $\gamma_{ph}^{L,R}$ as nuisance parameters with best-fit values of 1 and the deviations $\delta\gamma_{ph}^{L,R} = 0.15$. In the case where only a lower limit on the experimental $\log ft$ is known, the corresponding quadratic term in χ^2 is replaced by $[\max(0, \log ft^{th} - \log ft^{exp})/\delta \log ft^{exp}]^2$, i.e.,

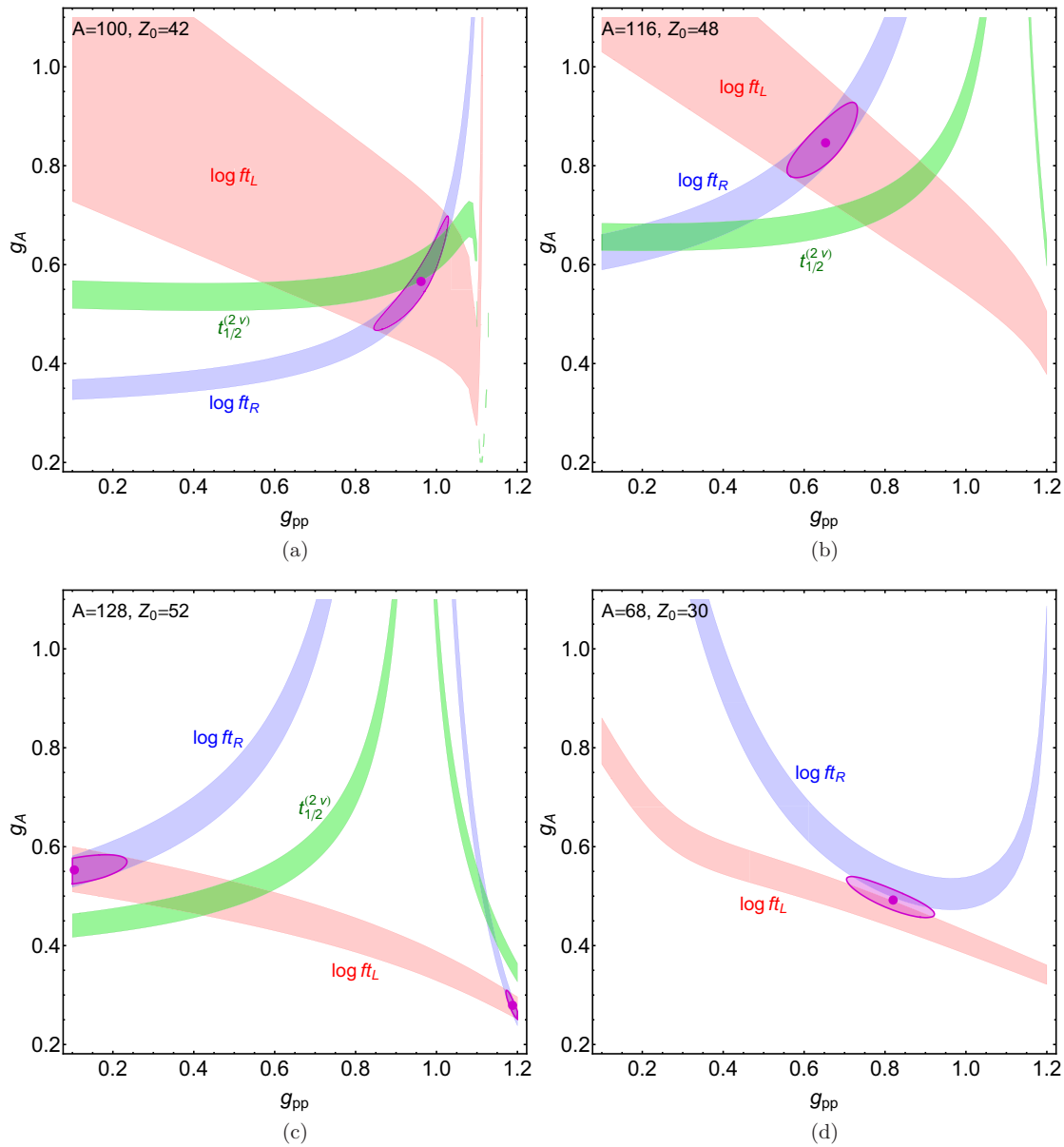

FIG. 4. Fitting g_A and g_{pp} in selected isobar triplets: $(A,Z_0) = (100,42)$ (a), (116,48) (b), (128,52) (c), and (68,30) (d). The light-shaded red and blue bands correspond to the individual 1σ constraint from the measurement of left-leg and right-leg β/EC decay, respectively, using the simplified χ^2 in Eq. (8). The dark purple area gives the combined 1σ parameter area with the dot denoting the best fit. The first three examples contain a measured $2\nu\beta\beta$ decaying isotope and the green band gives the corresponding parameter space. In addition to the experimental errors from Tables I, II, and III, a common theoretically induced error of 10% in the respective observables is included.

a single-sided exponential to represent the lower limit. Finally, the MCMC fit is performed using the fitness function $P = \exp(-\chi^2/2)$.

With two (non-nuisance) parameters and two constraints, the system is exactly determined and a solution with $\chi^2 = 0$ is generically expected. As is shown later, in some cases no consistent solution can be found for the given experimental data. As indicated by the curly brackets, for triplets in which the central isotope is even-even (i.e., identified by an odd Z_0), both decay legs are regulated by the same $g_{\rm ph}$ and thus the fit is performed with only one nuisance term and $\gamma^L_{\rm ph} = \gamma^R_{\rm ph}$.

Before discussing the results of the numerical fits, we would like to illustrate how the experimental data constrains $(g_A, g_{\rm pp})$ in a few examples. By omitting the nuisance parameters and shifting their induced uncertainty into a theoretical error on the $\log ft$, Eq. (7) simplifies to

$$\chi^2(g_A, g_{\rm pp}) = \frac{\left(\log ft^{\rm th}_L(g_A, g_{\rm pp}) - \log ft^{\rm exp}_L\right)^2}{\left(\delta \log ft^{\rm exp}_L\right)^2 + (\delta \log ft^{\rm th})^2} + \frac{\left(\log ft^{\rm th}_R(g_A, g_{\rm pp}) - \log ft^{\rm exp}_R\right)^2}{\left(\delta \log ft^{\rm exp}_R\right)^2 + (\delta \log ft^{\rm th})^2}, \quad (8)$$

resulting in a two-dimensional parameter space that can be easily visualized. Figure 4 shows the χ^2 fit based on Eq. (8) and the individual contributions from the measurement of the left-leg (red) and right-leg (blue) β/EC decays. In addition to the experimental errors, the χ^2 fit includes a common theoretical uncertainty of $\delta \log ft^{\rm th} = 10\%$. It has been chosen to be rather unrealistically small to show the effect of the experimental errors that otherwise are usually small compared to the model uncertainty. In the first three cases $(A, Z_0) = (100,42)$ [Fig. 4(a)], (116,48) [Fig. 4(b)], and (128,52) [Fig. 4(c)], the triplet includes a $2\nu\beta\beta$-decay isotope for which the half-life has been measured, $^{100}_{42}$Mo, $^{116}_{48}$Cd, and $^{128}_{52}$Te, respectively. The green band gives the correspondingly allowed 1σ parameter space. For $^{100}_{42}$Mo (a) it overlaps well with the fit from the β/EC decays. In the other two cases [Figs. 4(b) and 4(c)], there is a tension between single-β/EC decay and $2\nu\beta\beta$-decay data in the chosen model, but in both cases the discrepancy corresponds to a modest difference in g_A, by less than 30%. We discuss this discrepancy and possible causes at the end of Sec. III C. In the $A = 128$ case [Fig. 4(c)], there are formally two best-fit solutions, the significance of which we comment on below. The final scenario [Fig. 4(d)] illustrates a case where there is a tension between experimental data and theoretical predictions; i.e., the minimal χ^2 is different from zero.

For the actual numerical determination of the best-fit parameters and their errors, we use Eq. (7), where we include a 15% uncertainty in the value(s) of the particle-hole nuisance parameter(s) $g_{\rm ph}$ to model an additional theoretical uncertainty. Using the MCMC method described above, we determine the best-fit values and 1σ errors for $g^{\rm fit}_{\rm pp}$ and $g^{\rm fit}_A$ in all triplets as given in Tables I and II. They are based on the fully marginalized distribution for the given parameter, but we omit secondary solutions for large $g_{\rm pp}$ beyond the divergence, cf. Fig. 4(c). These large values of $g_{\rm pp}$ make the pnQRPA solutions unstable and in the worst case the whole set of pnQRPA solutions collapses because the condition of small-amplitude motion of the RPA theory becomes seriously violated [35].

In Tables I and II, the results highlighted with italic numbers correspond to fitting results with a minimal χ^2 value of the order of 1, indicating a slight tension between the experimental data and the theoretical predictions. As an example, the fitting of triplet $A = 68$, $Z_0 = 30$ is illustrated in Fig. 4(d). While the numerical fit in Table I includes a larger theoretical uncertainty from the variation of the left- and right-leg particle-hole parameters $\gamma^{L,R}_{\rm ph}$, this is not sufficient to achieve a vanishing $\chi^2_{\rm min}$. Similar behavior occurs for the other triplets highlighted with italic numbers in the table. In such cases, the statistical uncertainty likely underestimates the true theoretical error.

For the triplets $A = 80$, $Z_0 = 35$ and $A = 130$, $Z_0 = 54$, the minimal χ^2 value is substantially different from zero ($\chi^2_{\rm min} = 33$ and 15, respectively), meaning that there is a large

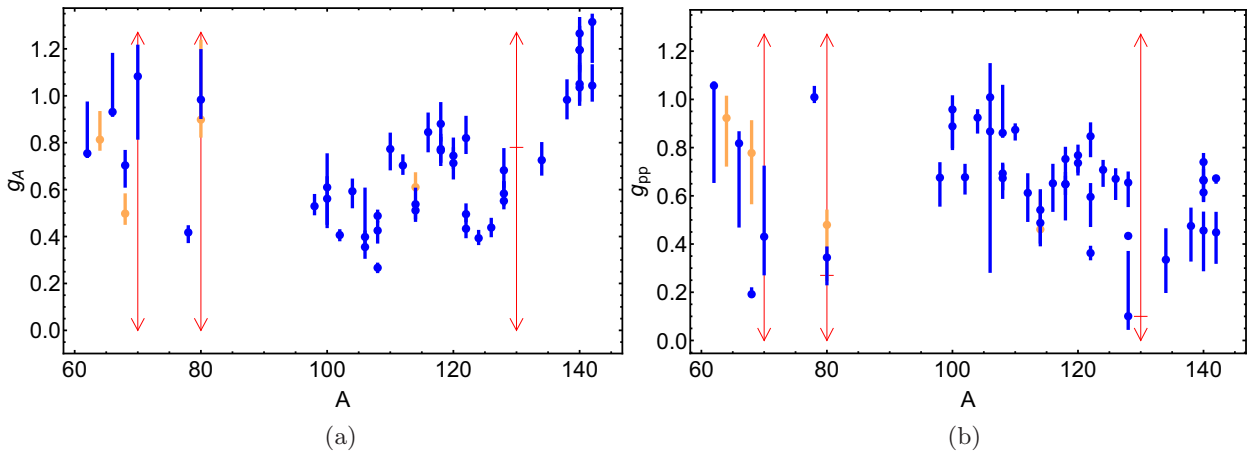

FIG. 5. g_A (a) and $g_{\rm pp}$ (b) determined in the individual triplet fits as a function of the mass number A, cf. Tables I and II. The error bars denote the 1σ parameter ranges. The dark blue and light orange values correspond to triplet fits with best fit solution $\chi^2_{\rm min} = 0$ (within numerical tolerance) and ≈ 1, respectively. The horizontal lines and associated vertical double arrows indicate fits with a strong tension with data where no meaningful error could be determined.

tension. We still give the nominal best-fit values for g_A and g_{pp}, highlighted in bold in these cases, to indicate the tendency of the fit, but we do not quote an uncertainty. In fact, in both cases the best fit is achieved at the limit of the considered parameter space and the statistical uncertainty is rather meaningless. Finally, for $A = 70$, $Z_0 = 29$ no meaningful fit was achieved. In all other cases, a minimal $\chi^2 = 0$ (within numerical tolerance) was found. As can be seen in Tables I and II, problems to fit the experimental data mostly occur for lighter nuclei with $A \leqslant 80$. This could indicate the diminishing flexibility of the *pn*QRPA model in going from the heavy nuclei, with large active single-particle model spaces, towards the lighter nuclei with small active model spaces, better suited for shell-model description.

The results are also graphically illustrated in Fig. 5, as a function of the mass number A. Analogous to the tables, the light orange points and 1σ error bars represent triplet fits with $\chi^2_{\min} \approx 1$ whereas the blue points correspond to $\chi^2_{\min} = 0$ (within numerical tolerance). The vertical double arrows (and horizontal lines for the nominal best fit, where applicable) indicate the cases with a strong tension with data as discussed above. As seen in the plots, the best-fit values in these scenarios are still in the right ballpark of the neighboring fits.

The strongest feature in the plots is the rise of g_A with larger A from $A = 98$ to 142 accompanied with a fall of g_{pp}. In this region the effective g_A increases from a strongly quenched $g_A \approx 0.4$ around $A = 100$ to an essentially unquenched $g_A \approx 1.1$ around $A = 140$. Although there is a considerable spread in the values, the fitting results of triplets within the same mass number A are largely compatible, illustrated by the overlapping error bars in Fig. 5. The tendency for lighter nuclei ($A = 80$ and below) is less clear and here the result is also affected by the large number of cases with tension to data. The tendency of a growing effective value of g_A with mass number for the $A \geqslant 100$ nuclei is in agreement with the linear model of Ref. [48]. From Fig. 5(a) one can deduce the average value of $g_A \approx 0.6$ for the $A \geqslant 100$ nuclei in accordance with the analysis of Ref. [48].

Using the thus-fitted parameters, we calculate the predicted $2\nu\beta\beta$ decay half-lives for all relevant isotopes as listed in Table III under $[t^{(2\nu)}_{1/2}]_{\text{triplet}}$. The calculation includes the correlation among g_A, g_{pp}, and g_{ph}; i.e., we use the full probability density from the MCMC fit. Confirming the expectation of the simple two-dimesional fits shown in Fig. 4, the measured $2\nu\beta\beta$-decay half-life of ^{100}Mo is consistent with the prediction within 1σ. On the other hand, the predictions for ^{116}Cd and ^{128}Te are too small by a factor of about 2 compared to the experimental results. We further discuss this discrepancy at the end of the next section. According to the calculated half-lives, the $2\nu\beta\beta$ decay of the nucleus ^{110}Pd would be an interesting case to measure in the future.

C. Fitting isobaric multiplets

Under the assumption that g_A is a function of the mass number A only, as justified in the Introduction, we can extend the analysis of individual triplets by fitting all β/EC decays within a system (multiplet) of isobaric isotopes. This allows us to incorporate the full experimental information available. On the other hand, we endeavor to include the full parametric uncertainty inherent in the *pn*QRPA models used in this study. This means that for each isobaric multiplet we use a common g_A and a set of (g_{pp}, g_{ph}) for each even-even isotope within the multiplet. The resulting multiplets are listed in Table IV, identified by (A, Z_0) of the first isotope. The table indicates

TABLE IV. Isobaric multiplets of β^+/EC and β^- decaying isotopes studied in the present article. An isobaric multiplet is identified by the mass number A and the lowest atomic number Z_0 among its isotopes. The individual isotopes are indicated with their atomic number and the arrows denote the direction of the relevant β^+/EC decays. The column "DOF" gives the degrees of freedom, i.e., the number of free parameters (one g_A and a g_{pp} for each even-even isotope) minus the number of experimental constraints. $2\nu\beta\beta$ decaying isotopes are underlined. The values of g_A are determined in the isobar fits described in Sec. III C. Cases in which the best-fit $\chi^2_{\min}$ is in the range [0.8, 1.5], indicating slight tension with data, are highlighted with italic numbers. Cases with stronger tension are highlighted in bold. In all other cases a $\chi^2_{\min}$ of the order expected by the degrees of freedom was found.

A	Z_0	Multiplet	DOF	g_A^{fit}
62	28	28 ← 29 ← 30	3-2	$0.80^{+0.43}_{-0.01}$
64	28	28 ← 29 → 30	3-2	$0.90^{+0.11}_{-0.09}$
66	28	28 → 29 → 30	3-2	$1.00^{+0.19}_{-0.16}$
68	29	29 → 30 ← 31 ← 32	3-3	$0.65^{+0.06}_{-0.07}$
70	29	29 → <u>30</u> ← 31 → 32	3-3	
78	34	34 ← 35 → 36	3-2	$0.35^{+0.59}_{-0.02}$
80	33	33 → <u>34</u> ← 35 → 36 ← 37	3-4	**1.40**
98	39	39 → 40 → 41	2-2	$0.53^{+0.04}_{-0.03}$
100	41	41 → <u>42</u> ← 43 → 44	3-3	$0.37^{+0.22}_{-0.00}$
102	42	42 → 43 → 44	3-2	$0.34^{+0.16}_{-0.00}$
104	44	<u>44</u> ← 45 → 46	3-2	$0.59^{+0.28}_{-0.10}$
106	45	45 → 46 ← 47 → 48	3-3	$0.40^{+0.02}_{-0.02}$
108	44	44 → 45 → 46 ← 47 → 48	4-4	$\mathit{0.41}^{+0.01}_{-0.01}$
110	46	<u>46</u> ← 47 → 48	3-2	$0.71^{+0.38}_{-0.13}$
112	48	48 ← 49 → 50	3-2	$0.67^{+0.19}_{-0.03}$
114	46	46 → 47 → <u>48</u> ← 49 → 50	4-4	$\mathit{0.60}^{+0.03}_{-0.03}$
116	48	<u>48</u> ← 49 → 50	3-2	$0.68^{+0.38}_{-0.01}$
118	48	48 → 49 → 50 ← 51 ← 52	4-4	$0.75^{+0.06}_{-0.04}$
120	48	48 → 49 → 50 ← 51	3-3	$0.71^{+0.06}_{-0.05}$
122	48	48 → 49 → <u>50</u> | 52 ← 53 ← 54 ← 55	5-5	$\mathit{0.49}^{+0.03}_{-0.03}$
124	54	54 ← 55 ← 56	3-2	$0.34^{+0.20}_{-0.02}$
126	54	54 ← 55 ← 56	3-2	$0.35^{+0.20}_{-0.02}$
128	52	<u>52</u> ← 53 → 54 ← 55 ← 56	4-4	$\mathit{0.59}^{+0.05}_{-0.06}$
130	54	54 ← 55 → 56	3-2	**0.78**
134	56	56 ← 57 ← 58	3-2	$0.72^{+0.10}_{-0.08}$
138	58	58 ← 59 ← 60	3-2	$0.92^{+0.20}_{-0.09}$
140	58	58 ← 59 ← 60 ← 61 ← 62 ← 63 ← 64	5-6	$1.10^{+0.07}_{-0.09}$
142	60	60 ← 61 ← 62 ← 63	3-3	$1.20^{+0.07}_{-0.12}$

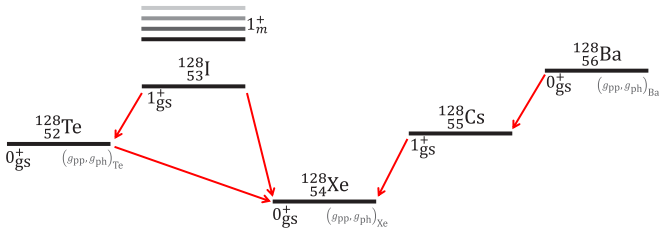

FIG. 6. Decay scheme for isotopes in the isobaric quintet $A = 128$, $Z = 52$–56. The different parameters g_{pp} and g_{ph} used in the fit for this multiplet are indicated for each even-even isotope in the system. Together with g_A, this leads to four (non-nuisance) parameters compared to four constraints from the β/EC decays. The system also contains the $2\nu\beta\beta$ isotope $^{128}_{52}$Te decaying to $^{128}_{54}$Xe.

all isotopes in the multiplet by their atomic number and the arrows give the direction of the decays. The multiplicity within the isobaric systems ranges from three to seven isotopes. The triplets are obviously identical to the ones discussed in the previous section but we would like to note that we now allow for more parametric freedom because we use a separate g_{pp} for each even-even isotope. Almost all triplets contain two even-even isotopes, i.e., two different g^L_{pp} and g^R_{pp} are used in the fit. Only the triplet (98,39) contains a single even-even isotope and the fit performed is identical to the one in the previous section.

In general, the degree of freedom in a fit is given by the number of free parameters (one g_A and a g_{pp} for each even-even isotope) minus the number of experimental constraints (number of measured β/EC decays). This difference is given in Table IV under "DOF", indicating that we encounter underconstrained (DOF > 0), exactly constrained (DOF $= 0$), and overconstrained (DOF < 0) systems. While we also include a g_{ph} for each even-even isotope, this does not change the number of degrees of freedom because the g_{ph} is treated as a nuisance parameter. An example of the decays and parameters involved is shown in Fig. 6 in the case of the multiplet (128,52).

The MCMC fitting procedure is analogous to the triplet case with a χ^2 function of the form of Eq. (7): there is a contribution for each observable (β/EC decay), with the theoretically calculated log ft values depending on the appropriate g^i_{pp} and γ^i_{ph} and the global g_A. In addition, there is a nuisance term for each of the particle-hole parameters γ^i_{ph} where we again use an uncertainty of $\delta\gamma^i_{ph} = 0.15$. As before, we use the experimental measurements and errors of the β/EC decay log ft values from Tables I and II.

An example of the result of an isobar fit is shown in Fig. 7 displaying the probability density functions in three different marginalized parameter planes as derived in the isobaric system (100,41) containing the $2\nu\beta\beta$-decay isotope $^{100}_{42}$Mo. It is a quartet with two even-even isotopes and thus described by the following three parameters, g_A, g^{Mo}_{pp}, and g^{Ru}_{pp}, and two nuisance parameters, γ^{Mo}_{ph} and γ^{Ru}_{ph}. The system is exactly constrained and consistent; thus the minimal χ^2 is zero. Nevertheless, there is a sizable uncertainty and especially the parameter g^{Ru}_{pp} can vary strongly and no lower limit can be determined at 2σ within the chosen parameter range. In this case the two particle-particle parameters can be very different. For example, the combination $g^{Mo}_{pp} \approx 0.7$ and $g^{Ru}_{pp} \approx 0.1$ is allowed by the combined experimental data within 2σ. Another consequence of this is that g_A is effectively suppressed compared to the triplet fit because lower values are statistically preferred for small g^{Ru}_{pp}. The experimental log ft errors and the variation of γ^{Mo}_{ph} and γ^{Ru}_{ph} provide an additional source of uncertainty.

The results of the fits are displayed in Table IV, which lists the best-fit values and 1σ uncertainties of g_A for all multiplets. As in the case of the individual triplets, italicized values denote multiplets in which there is a slight tension between the combined experimental data and the theoretical predictions. Comparing with Tables I and II, the tension for $A = 62$ and 80 is resolved by introducing the additional freedom in the multiplet fits. On the other hand, the multiplets $A = 108$, 114, 122, and 128 exhibit slight tension, due to the larger number

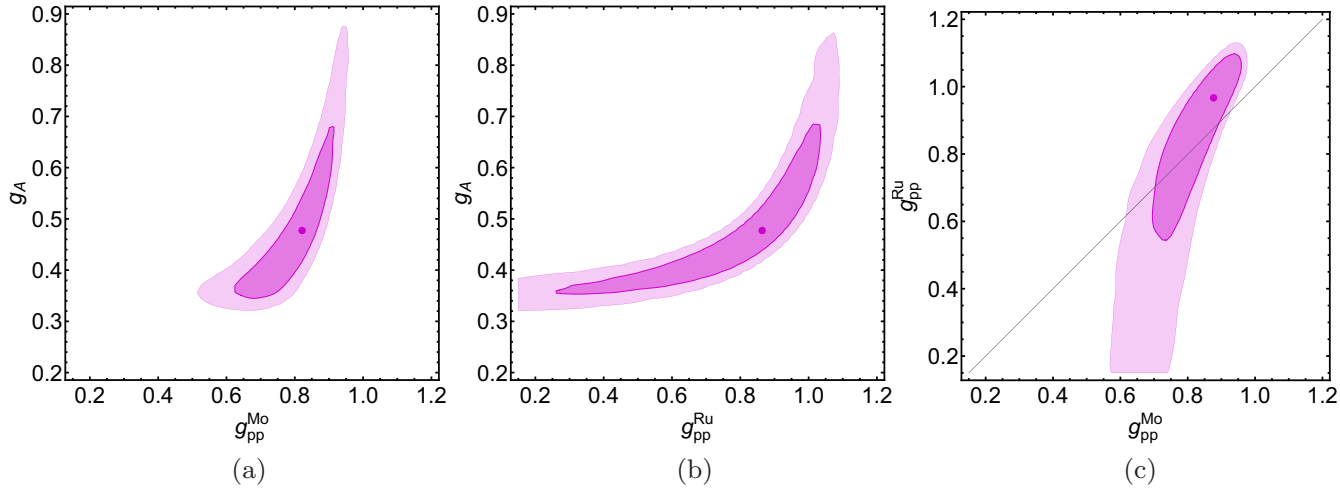

FIG. 7. Probability density function for the fit of the isobaric system $A = 100$, $Z_0 = 41$ in three marginalizations of the parameter space: $g_A - g^{Mo}_{pp}$ (a), $g_A - g^{Ru}_{pp}$ (b), and $g^{Mo}_{pp} - g^{Ru}_{pp}$ (c). The colored areas denote the 1σ and 2σ extents of the parameter space and the dot denotes the maximum.

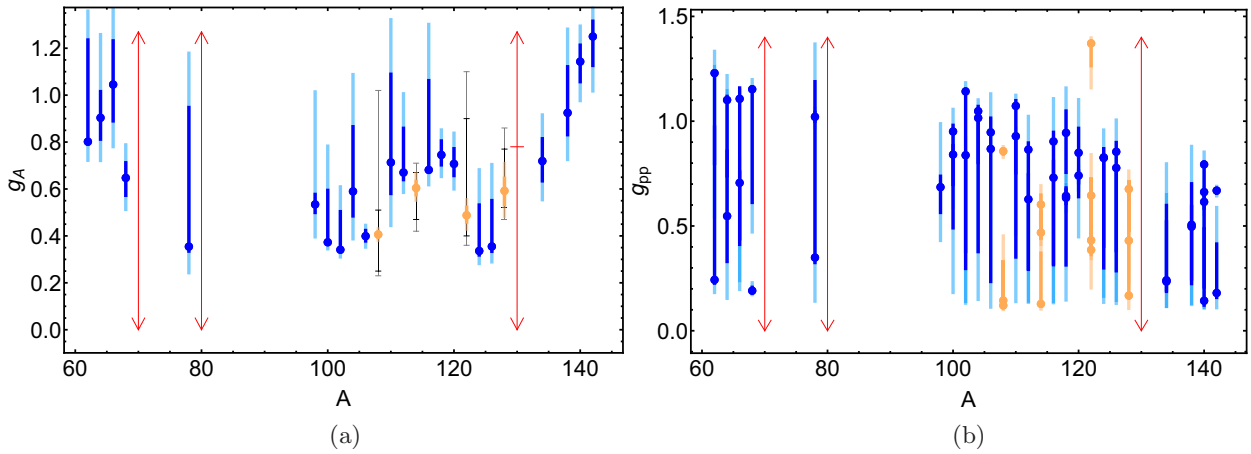

FIG. 8. g_A (a) and g_{pp} (b) determined in the isobaric multiplet fits as a function of the mass number A, cf. Table IV. The error bars denote the 1σ and 2σ parameter ranges. The blue values correspond to multiplets with a best-fit solution as expected by the degrees of freedom, whereas light orange values denote a slight tension with $\chi^2_{\text{min}} \approx 1$. In these cases, the underlying black and gray error lines give the 1σ and 2σ range among the triplet fits, respectively, for comparison. The horizontal lines and associated vertical double arrows indicate fits with a strong tension where no meaningful error could be determined.

of simultaneous constraints that dominate over the additional freedom. The strong tension for $A = 70$, 80, and 130 remains in the multiplet approach.

The results are also graphically displayed in Fig. 8(a), where we plot the extracted values of g_A as a function of the mass number A, also showing the 1σ and 2σ uncertainties. It can be directly compared to Fig. 5(a), and it can be seen that the general behavior exhibited is similar in the two plots. Due to the combined fit of all isobaric nuclei, the dependence on A is smoother in Fig. 8(a), albeit with sometimes considerable uncertainty for some multiplets, suggesting a systematic dependence of g_A with the mass number A within the range $98 \leqslant A \leqslant 142$. The multiplets $A = 108$, 114, 122, and 128 with slight tension correspond to triplets with comparatively large differences in the fitted g_A values. This tension between the triplet g_A values leads to a worse fit when combining within a multiplet and the resulting uncertainty likely underestimates the true error in g_A. For comparison in these cases, Fig. 8(a) also shows the 1σ and 2σ range derived in the associated triplet fits (i.e., the minimal and maximal extent in g_A among all triplets at the given uncertainty). This likely provides a more realistic estimate of the uncertainty in g_A.

Figure 8(b) shows g_{pp} as a function of A within the isobaric fits where each dot represents the best-fit point of an individual g^i_{pp}. As is illustrated in Fig. 7 and discussed above, the freedom of allowing a different g_{pp} per even-even isotope introduces a degeneracy where individual g_{pp} can vary strongly. Figure 8(b) demonstrates that in almost all cases at least one of the g_{pp} can be small, hitting the limit of the chosen variable range. As a result the apparent spread among the g_{pp} is large and there is only a tendency of squeezing the range to lower values for increasing A. It should be kept in mind that the fitting procedure also means that the individual g_{pp} values are correlated to satisfy the experimental constraints. Despite the large freedom and large variability of the g^i_{pp} it is remarkable that the corresponding uncertainty of g_A remains comparatively small. This could indicate a robustness of the underlying *pn*QRPA-based nuclear-structure calculations against parameter variations.

Using the thus-fitted parameters, we calculate the predicted $2\nu\beta\beta$-decay half-lives for all relevant isotopes as listed in Table III under $[t^{(2\nu)}_{1/2}]_{\text{multiplet}}$. The calculation includes the correlation among the parameters g_A, g^i_{pp}, and γ^i_{ph}; i.e., we use the full probability density from the MCMC fit. Unfortunately, many of the $2\nu\beta\beta$ isotopes are part of multiplets with a slight or severe tension between experimental data and theoretical prediction of the EC/β-decay fit. These are highlighted in Table III as usual. The uncertainties quoted in these cases are likely underestimates. The multiplet fits incorporating ^{116}Cd and ^{128}Te are not able to relax the tension with the measured $2\nu\beta\beta$-decay half-lives in these isotopes.

On the other hand, in the analysis carried out in Ref. [26] a very weakly decreasing A dependence was obtained for the effective value of g_A in the IBA-2 and ISM frameworks. The result was based on the comparison of the computed and experimental half-lives of the $2\nu\beta\beta$ decays. This weak trend is in line with the analysis of Ref. [48] where it was observed that the constant $g_A = 0.6$ reproduces better the measured $2\nu\beta\beta$ half-lives than the growing trend for g_A obtained by the β-decay analysis (see Table VI of Ref. [48]). In fact, having a look at Fig. 4 as well as Table III of this work, in both the triplet and multiplet analyses a decreasing multiplicative factor of g_A, as a function of the mass number A, would bring the computed half-lives closer to the measured ones. The fact that the analyses of the β decays and the $2\nu\beta\beta$ decays give opposite trends is a sign that there are basic differences between the two modes of decay. One difference is that for the $2\nu\beta\beta$ decays more than one low-lying state can contribute and the contribution coming from the first virtual 1^+ state of the intermediate nucleus does not exhaust the whole $2\nu\beta\beta$ NME (see Table V of Ref. [48]). The balance between the first contribution and the rest depends on the value of g_{pp} in a *pn*QRPA calculation, and the correlations of g_A and g_{pp} are most likely different for the β and $2\nu\beta\beta$ decays.

IV. CONCLUSIONS

In this work we studied single-β^+/EC and β^- decays for a number of isobaric triplets and more complicated isobaric chains of nuclei in the framework of the proton-neutron quasiparticle random-phase approximation.

The present calculations have been done with G-matrix-based two-nucleon interactions. By letting the value of the axial-vector coupling constant g_A vary freely, together with the particle-particle interaction strength parameter $g_{\rm pp}$, we have performed MCMC-based statistical analyses to chart the effective values of g_A in pnQRPA-based nuclear-structure calculations. Within the statistical fits of complete isobaric chains of nuclei we incorporated full parametric uncertainty of the nuclear model by using independent $g_{\rm pp}$ per even-even isotope as well as an uncertainty in the particle-hole parameter $g_{\rm ph}$. We thus not only confirm previous results of an apparent quenching of g_A in an extended analysis but we also provide a realistic estimate of the parametric uncertainty inherent in the nuclear model. This is important, also, to compare with other theory frameworks.

These findings may have some bearing on the studies of the contributions of the low-lying 1^+ intermediate states to the highly interesting $0\nu\beta\beta$ NMEs. The relation of our present results to the values of the $0\nu\beta\beta$ NMEs remains still an open issue but we view the present study as an incentive to tackle these issues in future investigations.

ACKNOWLEDGMENTS

This work was supported by the Academy of Finland under the Finnish Center of Excellence Program 2012–2017 (Nuclear and Accelerator Based Program at JYFL) and by the UK Royal Society International Exchanges Grant No. IE130084.

[1] J. Suhonen and O. Civitarese, Weak-interaction and nuclear-structure aspects of nuclear double beta decay, Phys. Rep. **300**, 123 (1998).
[2] J. Vergados, H. Ejiri, and F. Šimkovic, Theory of neutrinoless double beta decay, Rep. Prog. Phys. **75**, 106301 (2012).
[3] F. F. Deppisch, M. Hirsch, and H. Päs, Neutrinoless double-beta decay and physics beyond the standard model, J. Phys. G: Nucl. Part. Phys. **39**, 124007 (2012).
[4] W. Rodejohann, Neutrino-less double beta decay and particle physics, Int. J. Mod. Phys. E **20**, 1833 (2011).
[5] F. F. Deppisch, J. Harz, W.-C. Huang, M. Hirsch, and H. Päs, Falsifying high-scale baryogenesis with neutrinoless double beta decay and lepton flavor violation, Phys. Rev. D **92**, 036005 (2015); F. F. Deppisch, J. Harz, and M. Hirsch, Falsifying High-Scale Leptogenesis at the LHC, Phys. Rev. Lett. **112**, 221601 (2014).
[6] F. Deppisch, H. Päs, and J. Suhonen, Double beta decay versus cosmology: Majorana *CP* phases and nuclear matrix elements, Phys. Rev. D **72**, 033012 (2005).
[7] J. Suhonen and O. Civitarese, Review of the properties of the $0\nu\beta^-\beta^-$ nuclear matrix elements, J. Phys. G: Nucl. Part. Phys. **39**, 124005 (2012).
[8] J. Suhonen and O. Civitarese, Double-beta-decay nuclear matrix elements in the QRPA framework, J. Phys. G: Nucl. Part. Phys. **39**, 085105 (2012).
[9] J. Suhonen and O. Civitarese, Effects of orbital occupancies on the neutrinoless $\beta\beta$ matrix element of ^{76}Ge, Phys. Lett. B **668**, 277 (2008).
[10] J. Suhonen and O. Civitarese, Effects of orbital occupancies and spin-orbit partners on $0\nu\beta\beta$-decay rates, Nucl. Phys. A **847**, 207 (2010).
[11] J. Suhonen, Effects of orbital occupancies and spin-orbit partners II: $0\nu\beta\beta$ decays of ^{76}Ge, ^{82}Se and ^{136}Xe to first excited 0^+ states, Nucl. Phys. A **853**, 36 (2011).
[12] J. Barea and F. Iachello, Neutrinoless double-β decay in the microscopic interacting boson model, Phys. Rev. C **79**, 044301 (2009).
[13] R. Álvarez-Rodríguez, P. Sarriguren, E. Moya de Guerra, L. Pacearescu, A. Faessler, and F. Šimkovic, Deformed quasiparticle random phase approximation formalism for single- and two-neutrino double β decay, Phys. Rev. C **70**, 064309 (2004).
[14] E. Caurier, F. Nowacki, and A. Poves, Nuclear-structure aspects of the neutrinoless $\beta\beta$-decays, Eur. Phys. J. A **36**, 195 (2008).
[15] J. Menéndez, A. Poves, E. Caurier, and F. Nowacki, Disassembling the nuclear matrix elements of neutrinoless $\beta\beta$ decay, Nucl. Phys. A **818**, 139 (2009).
[16] T. R. Rodríguez and G. Martínez-Pinedo, Energy Density Functional Study of Nuclear Matrix Elements for Neutrinoless $\beta\beta$ Decay, Phys. Rev. Lett. **105**, 252503 (2010).
[17] A. Faessler, G. L. Fogli, E. Lisi, V. Rodin, A. M. Rotunno, and F. Šimkovic, Overconstrained estimates of neutrinoless double beta decay within the QRPA, J. Phys. G: Nucl. Part. Phys. **35**, 075104 (2008).
[18] J. Suhonen and O. Civitarese, Probing the quenching of $g_{\rm A}$ by single and double beta decays, Phys. Lett. B **725**, 153 (2013).
[19] J. D. Holt and J. Engel, Effective double-β-decay operator for ^{76}Ge and ^{82}Se, Phys. Rev. C **87**, 064315 (2013).
[20] J. Suhonen and O. Civitarese, Single and double beta decays in the $A = 100$, $A = 116$ and $A = 128$ triplets of isobars, Nucl. Phys. A **924**, 1 (2014).
[21] D. S. Delion and J. Suhonen, Effective axial-vector strength and β-decay systematics, Europhys. Lett. **107**, 52001 (2014).
[22] B. H. Wildenthal, M. S. Curtin, and B. A. Brown, Predicted features of the beta decay of neutron-rich sd-shell nuclei, Phys. Rev. C **28**, 1343 (1983).
[23] G. Martínez-Pinedo, A. Poves, E. Caurier, and A. P. Zuker, Effective g_A in the pf shell, Phys. Rev. C **53**, R2602(R) (1996).
[24] J. Menéndez, D. Gazit, and A. Schwenk, Chiral Two-Body Currents in Nuclei: Gamow-Teller Transitions and Neutrinoless Double-Beta Decay, Phys. Rev. Lett. **107**, 062501 (2011).
[25] E. Caurier, F. Nowacki, and A. Poves, Shell model description of the $\beta\beta$ decay of ^{136}Xe, Phys. Lett. B **711**, 62 (2012).
[26] J. Barea, J. Kotila, and F. Iachello, Nuclear matrix elements for double-β decay, Phys. Rev. C **87**, 014315 (2013).
[27] P. Vogel and M. R. Zirnbauer, Suppression of the Two-Neutrino Double-Beta Decay by Nuclear-Structure Effects, Phys. Rev. Lett. **57**, 3148 (1986).
[28] O. Civitarese, A. Faessler, and T. Tomoda, Suppression of the two-neutrino double β decay, Phys. Lett. B **194**, 11 (1987).
[29] J. Suhonen, Nuclear matrix elements of $\beta\beta$ decay from β-decay data, Phys. Lett. B **607**, 87 (2005).

[30] J. Suhonen, On the double-beta decays of ^{70}Zn, ^{86}Kr, ^{94}Zr, ^{104}Ru, ^{110}Pd and ^{124}Sn, Nucl. Phys. A **864**, 63 (2011).

[31] V. A. Rodin, A. Faessler, F. Šimkovic, and P. Vogel, Assessment of uncertainties in QRPA $0\nu\beta\beta$-decay nuclear matrix elements, Nucl. Phys. A **766**, 107 (2006).

[32] M. Kortelainen and J. Suhonen, Improved short-range correlations and $0\nu\beta\beta$ nuclear matrix elements of ^{76}Ge and ^{82}Se, Phys. Rev. C **75**, 051303(R) (2007).

[33] M. Kortelainen and J. Suhonen, Nuclear matrix elements of $0\nu\beta\beta$ decay with improved short-range correlations, Phys. Rev. C **76**, 024315 (2007).

[34] J. Suhonen and M. Kortelainen, Nuclear matrix elements for double beta decay, Int. J. Mod. Phys. E **17**, 1 (2008).

[35] J. Suhonen, *From Nucleons to Nucleus: Concepts of Microscopic Nuclear Theory* (Springer, Berlin, 2007).

[36] J. Suhonen, A. Faessler, T. Taigel, and T. Tomoda, Suppression of the β^+ decays of ^{148}Dy, ^{150}Er and ^{152}Yb, Phys. Lett. B **202**, 174 (1988).

[37] J. Suhonen, T. Taigel, and A. Faessler, *pn*QRPA calculation of the β^+/EC quenching for several neutron-deficient nuclei in mass regions $A = 94$–110 and $A = 146$–156, Nucl. Phys. A **486**, 91 (1988).

[38] J. Kotila and F. Iachello, Phase-space factors for double-β decay, Phys. Rev. C **85**, 034316 (2012).

[39] J. Hyvärinen and J. Suhonen, Nuclear matrix elements for $0\nu\beta\beta$ decays with light or heavy Majorana-neutrino exchange, Phys. Rev. C **91**, 024613 (2015).

[40] H. Ejiri, N. Soukouti, and J. Suhonen, Spin-dipole nuclear matrix elements for double beta decays and astro-neutrinos, Phys. Lett. B **729**, 27 (2014)

[41] M. Haaranen, P. C. Srivastava, and J. Suhonen, Forbidden nonunique β decays and effective values of weak coupling constants, Phys. Rev. C **93**, 034308 (2016).

[42] J. Hyvärinen and J. Suhonen, Analysis of the intermediate-state contributions to neutrinoless double β^- decays, Adv. High Energy Phys. **2016**, 4714829 (2016).

[43] A. Bohr and B. R. Mottelson, *Nuclear Structure* (Benjamin, New York, 1969), Vol. I.

[44] J. Suhonen, Calculation of allowed and first-forbidden beta-decay transitions of odd-odd nuclei, Nucl. Phys. A **563**, 205 (1993).

[45] A. Juodagalvis and D. J. Dean, Gamow-Teller GT_+ distributions in nuclei with mass $A = 90$–97, Phys. Rev. C **72**, 024306 (2005).

[46] A. Faessler, G. L. Fogli, E. Lisi, V. Rodin, A. M. Rotunno, and F. Šimkovic, Overconstrained estimates of neutrinoless double beta decay within the QRPA, arXiv:0711.3996v1.

[47] N. Yoshida and F. Iachello, Two-neutrino double-β decay in the interacting boson-fermion model, Prog. Theor. Exp. Phys. (2013) 043D01.

[48] P. Pirinen and J. Suhonen, Systematic approach to β and $2\nu\beta\beta$ decays of mass $A = 100$–136 nuclei, Phys. Rev. C **91**, 054309 (2015).

[49] J. Kotila, J. Suhonen, and D. S. Delion, Two-neutrino double beta decay of ^{76}Ge in an anharmonic vibrator approach, J. Phys. G: Nucl. Part. Phys. **36**, 045106 (2009).

[50] J. Kotila, J. Suhonen, and D. S. Delion, Description of the two-neutrino $\beta\beta$ decay of ^{100}Mo by *pn*MAVA, J. Phys. G: Nucl. Part. Phys. **37**, 015101 (2010).

[51] A. Bohr and B. R. Mottelson, *Nuclear Structure* (Benjamin, New York, 1975), Vol. II.

[52] A. Bohr and B. R. Mottelson, On the role of the δ resonance in the effective spin-dependent moments of nuclei, Phys. Lett. B **100**, 10 (1981).

[53] ENSDF at NNDC site, http://www.nndc.bnl.gov/.

[54] A. S. Barabash, Average and recommended half-life values for two neutrino double beta decay: Upgrade-2013, AIP Conf. Proc. **1572**, 11 (2013).

[55] W. H. Press, S. A. Teukolsky, W. T. Vetterling, and B. P. Flannery, *Numerical Recipes: The Art of Scientific Computing, Third Edition* (Cambridge University, Cambridge, England, 2007).